Plasmonic Metasurfaces Based on Nanopin-Cavity Resonator for Quantitative Colorimetric Ricin Sensing

Jiao-Rong Fan, Jia Zhu, Wen-Gang Wu, and Yun Huang*

In view of the toxic potential of a bioweapon threat, rapid visual recognition and sensing of ricin has been of considerable interest while remaining a challenging task up to date. In this study, a gold nanopin-based colorimetric sensor is developed realizing a multicolor variation for ricin qualitative recognition and analysis. It is revealed that such plasmonic metasurfaces based on nanopin-cavity resonator exhibit reflective color appearance, due to the excitation of standing-wave resonances of narrow bandwidth in visible region. This clear color variation is a consequence of the reflective color mixing defined by different resonant wavelengths. In addition, the colored metasurfaces appear sharp color difference in a narrow refractive index range, which makes them especially well-suited for sensing applications. Therefore, this antibody-functionalized nanopin-cavity biosensor features high sensitivity and fast response, allowing for visual quantitative ricin detection within the range of 10–120 ng mL^{-1} (0.15×10^{-9}–1.8×10^{-9} M), a limit of detection of 10 ng mL^{-1}, and the typical measurement time of less than 10 min. The on-chip integration of such nanopin metasurfaces to portable colorimetric microfluidic device may be envisaged for the quantitative studies of a variety of biochemical molecules.

1. Introduction

Ricin has been considered as a major bioterrorism weapon because of its natural high abundance, ready availability (extracted from castor bean plants), and high cytotoxicity in blocking protein synthesis and inducing cell death.[1,2] It has been found that a lethal level of the ricin in humans is about 5–10 μg kg^{-1} through inhalation or injection.[3,4] Even poisoned with the ricin in small doses, it can cause a state of coma in man for several weeks.[5] Additionally, there is as yet no approved antidote for the treatment of ricin poisoning.[6] Several recent ricin attacks have underscored the urgent and critical need for a fast and sensitive detection against ricin biothreat.[7] Some effective approaches, such as enzyme-linked immunosorbent assay (ELISA),[8,9] immunoassays,[10–12] mass spectrometric analysis,[13,14] electrochemiluminescence assay,[15] surface plasmon resonance detection,[16–18] and atomic force microscopy (AFM) recognition imaging,[19] have been widely reported in previous publications and have high performance in specificity and sensitivity. Most striking, the earliest colloidal gold particle-based ELISA methods has significantly improved assay times and has so far remained competitive in ricin detection sensitivity (limit of detection as low as 1 ng mL^{-1}).[8] Specifically, Xu and co-workers[19] modified gold-coated AFM tip with polyethylene glycol derivative to attach antiricin antibody for ricin recognition with the sensitivity up to fg mL^{-1}. However, since most of the current methods require time-consuming complex assay procedure, expensive instrumentation, and professional operator, a simple and novel method for the efficient detection of ricin is still necessary. Fortunately, colorimetric sensing is free of these problems, offering more flexibility for visual, real-time

Dr. J.-R. Fan, J. Zhu, Prof. W.-G. Wu, Dr. Y. Huang
National Key Laboratory of Science and Technology on Micro/Nano Fabrication
Institute of Microelectronics
Peking University
Beijing 100871, P. R. China
E-mail: wuwg@pku.edu.cn
Dr. J.-R. Fan, J. Zhu, Prof. W.-G. Wu, Dr. Y. Huang
Innovation Center for MicroNanoelectronics and Integrated System
Beijing 100871, P. R. China

DOI: 10.1002/smll.201601710

monitoring, and on-site detection of target molecule binding processes.

Current reported colorimetric sensors mostly based on plasmon-resonant nanoparticles have focused on multicolor changing phenomenon induced by the nanoparticle assembly during the molecular binding.[8,9,20–29] And yet, the nanoparticle cross-linked aggregation requires sufficiently dispersing, uniform shape and good stability, which greatly limit its utility. On the other hand, shape- and spacing-dependent metal-nanoparticle scattering colors have its limitations to generate a reasonable number of color variability and selectivity. Moreover, owing to strong radiative damping, the localized surface plasmon resonance of metal nanostructures generally exhibit broad resonance peaks, which reduce their colorimetric resolution and limit the performances of localized surface plasmon resonance (LSPR) sensors. Improved colorimetric systems that overcome these limitations would be highly desirable. We have recently reported the incident-orientation-dependent plasmonic pixels in dark-field mode based on helm-shaped nanoresonator, achieving a broad gamut of colors. We showed that such resonators exhibit multiple resonance peaks and narrow bandwidth in the visible range, which is clearly required for high-performance colorimetric sensing.[30]

Here, we report a plasmonic colorimetric sensing system based on plasmonic nanopin metasurfaces (PNPMs) for ricin quantitative recognition and analysis. Such patterned nanopin arrays are attractive due to their ability to generate bright-field reflective colors (**Figure 1**). The structural color can be broadly tailored across the visible spectrum by a sophisticated tuning of structural geometry. As discussed later, we will demonstrate that this highly ordered nanostructures can efficiently excite surface plasmons in standing-wave mode and produce clear color variation in a narrow refractive index range. Benefiting from this unique optical functionality of PNPMs, they provide a novel strategy for the implementation of visual and quantitative ricin recognition with good selectivity and sensitivity.

2. Results and Discussion

Inspired by scallop effect in Bosch process,[31,32] subwavelength periodic nanostructures were patterned by a combination of electron beam lithography and advanced silicon etch. The detailed process steps of fabrication are illustrated in structure fabrication section of Supporting Information. Prior to the metal deposition, the smooth silicon oxide layer covering the whole structures can be formed by thermal oxidation. Figure 1a shows a scanning electron microscope (SEM) image of the proposed 3D architectures. The structures consist of arrayed disk-capped nanopillars aligned in backplane with the gold nanocoating by angle-resolved metal deposition. In addition, to confirm the back-side gold coating of disk, we have prepared cross-section nanopin using focused ion beam in the Supporting Information (Figure S3). It is clearly seen that a large number of cavities are formed between the disks and the bottom film. The nanocavity can function as optical mirrors, by which the resonant confinement of visible light can be perpendicularly reflected back and forth to increase the reflection intensity, so that the electric field becomes the maximum at the ends and can form plasmonic standing-waves along the pillars.[33,34] With these characteristics of inherent coupled plasmon resonance and enhanced field confinement, narrow resonances of subwavelength cavity structures occurs in the visible range. Consequently, optical resonances of nanostructured transform incident white light to visible color, as illustrated in Figure 1b.

2.1. Color Generation and Refraction-Index Colorimetric Sensing

In order to understand the underlying physics, the numerical finite-difference time-domain (FDTD) analysis was performed to model plasmon response of nanopin-cavity structure. Calculated results of the reflectance and energy distributions of the relevant modes are shown in **Figure 2** for the specific structure arrays of periodicity p = 300 nm, diameter d = 220 nm, gold thickness t = 15 nm, and pillar height h = 100 nm. It can be seen that significant dips in reflection spectrum manifest multiple resonances. In Figure 2b,c, the electric-field and electric-charge intensity distributions clearly reveal the energy concentration mode of nanopin cavity at resonant wavelengths. Crucially, light can be reflected between two end surfaces of cavity, so

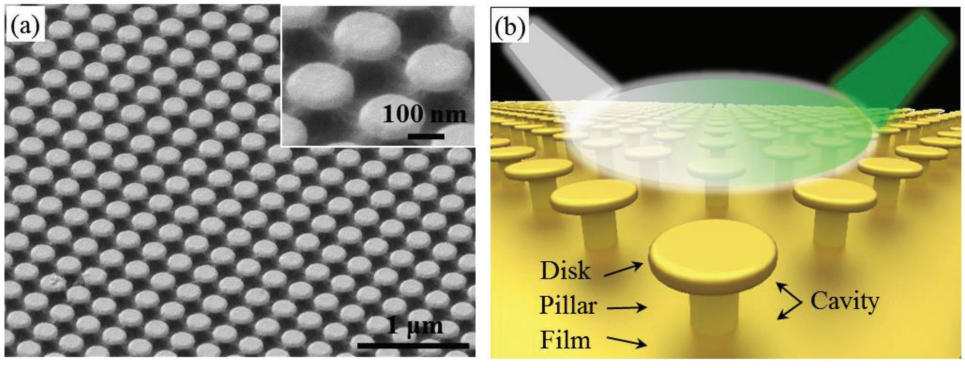

Figure 1. Surface plasmon metasurfaces and their structural coloration. a) A tilted view SEM image of the fabricated nanopin arrays. Inset: Magnified view of nanopin. b) Schematic diagram showing color creation of PNPMs. Incident white light is reflected back in visible color due to plasmon resonances in the plasmonic nanostructures.

DOI: 10.1002/smll.201601710

small NANO MICRO

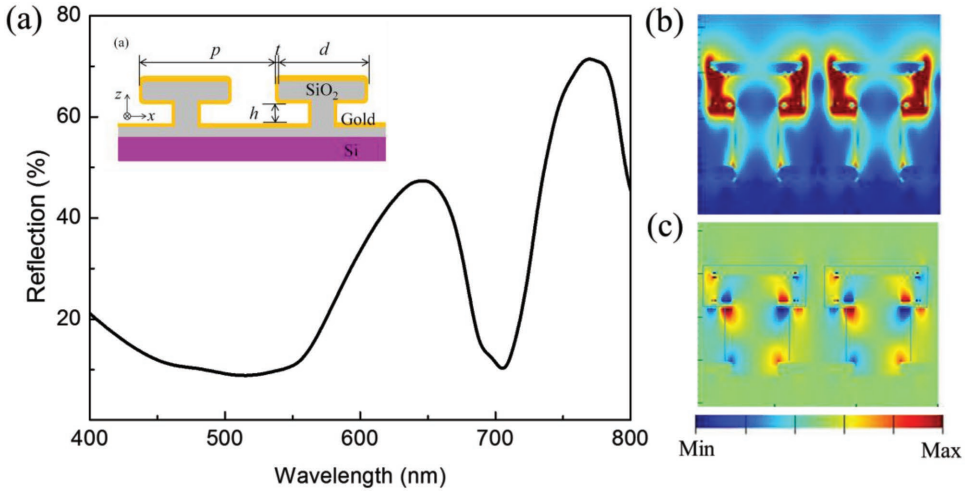

Figure 2. 3D-FDTD simulation of nanopin exhibiting coupled resonance modes. a) Calculated reflection spectrum with periodic boundary conditions. The dips are a sign of coupled resonances. Inset: Schematic of the simulation model. Normalized electric field b) and electric charge c) distributions, at a resonant wavelength of 701 nm, indicating significant electromagnetic field enhancement as well as surface plasmon resonances in nanopin cavity.

that the electric field can be greatly enhanced, resulting in high reflectance. The reflective optical flows in the cavity are shown in Movie S1 (Supporting Information). Furthermore, as can be seen from Figure 2c, the electric charges tend to accumulated along the pillar sidewall and top disk, indicating standing-wave surface plasmons of nanopin structure. As a result, our proposed nanocavity structure exhibits multispectral, narrow band, and high reflectance in visible wavelength (Figure 2a). These coupled resonances may lead to rich and subtle color selections through color mixing strategies, providing several advantages on the design and fabrication of colorimetric sensing device.

In this work, we patterned a chequerboard pattern with both diameter variations (d = 100–220 nm) and periodicity variations (p = 240–330 nm). **Figure 3**b and c show the measured results of their reflectance spectra with different values for d or p and their corresponding color appearances are presented in Figure 3a. SEM images of the fabricated nanopin samples are shown in Figure S2 (Supporting Information). Notably, for the indigo square (p = 300 nm, d = 220 nm), both the line shape and relative reflectance of the measured spectrum coincides well with the calculated one in Figure 2a. Varying structural parameters significantly affects their reflection spectra accompanied by drastically changes in plasmonic colors. One should also notice that multiple resonant peaks are observed with full width at half-maximum (fwhm) of less than 50 nm and the narrowing line shape is substantially conducive to saturated color selection.

Since the human eye has an instinctual perception for color variations in the 500–600 nm wavelength range. Therefore, the structure parameters have a stake in detection sensitivity and colorimetric resolution. Our proposed method offers good structure designing flexibility to achieve the maximum perceptible color change by a precise tuning of resonance location. To evaluate the colorimetric sensitivity of different arrays, we measure color response of our proposed structures under changing medium refractive indices (water: 1.33 and alcohol 1.36). **Figure 4** illustrates that arrays with p = 300 nm, d = 220 nm allow for larger color difference. Resonant dip-shift in the range of 550–600 nm is largely responsible for significant color variations, hence resulting

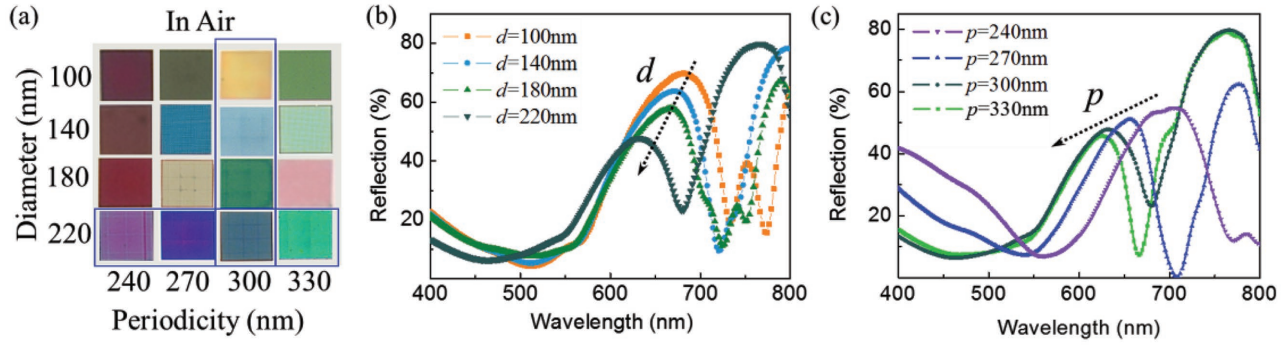

Figure 3. Designed structural layout corresponds to the noticeable plasmonic color, illustrating structure-dependent surface coloration. a) Bright-field microscope image of colorful chequerboard pattern. 20 × 20 μm^2 squares with predefined structural variations (d = 100–220 nm, p = 240–330 nm) result in a palette of reflective plasmonic colors. b,c) The measured reflection characteristics of plasmonic nanopin arrays with d and p varied individually.

DOI: 10.1002/smll.201601710

www.MaterialsViews.com

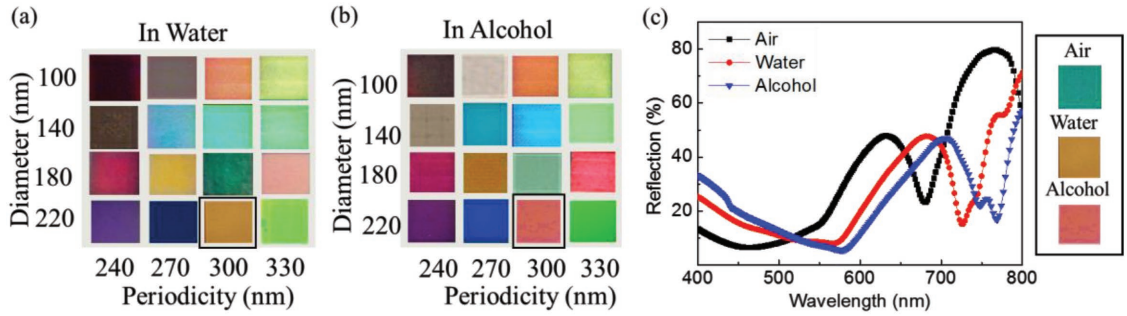

Figure 4. Colorimetric refractive index sensing with PNPMs. Color response to different aquatic medium: a) water 1.33 and b) alcohol 1.36. c) Measured reflection spectra as a function of refractive index for arrays $p = 300$ nm, $d = 220$ nm.

in the abundant transition colors as refraction index. It is an important metric to describe the high-resolution colorimetric sensing. In general, such plasmonic metasurfaces offer attractive possibilities to develop a high-performance colorimetric sensing device for characterizing biomolecular interactions. The application of well-designed nanopin metasurfaces for quantitative colorimetric ricin recognition will be demonstrated later.

2.2. Metasurface Functionalization

Figure 5a summarizes the procedure for fabricating antibody-functionalized biosensor surfaces. Step 1: Prior to linker deposition, the proposed metallic nanostructures were exposed to Piranha solution (H_2SO_4 and H_2O_2 with a volume ratio of 3:1) for 30 min, followed by rinsing in deionized water, and blow-dried under a stream of nitrogen. After this, a solution of 0.10×10^{-3} M 3,3′-dithiobis succinimidyl propionate (DSP) in dimethyl sulfoxide (DMSO) was added on the surface for 2 h at room temperature. We have used DSP to fabricate antibody-functionalized surfaces due to their short methylene chain for effective and efficient protein binding.[35] Step 2: The thiolate-based monolayer was chemisorbed on the gold surface functionalized with a terminal succinimide groups for further reaction, in a modified manner as previously described.[36] Step 3: 40 µL of a 0.1 mg mL^{-1} antibody against ricin (antiricin) solution was pipetted to the succinimide-modified gold substrate for 1 h. The antibody protein was immobilized through the amide linkage formed by the reaction of the terminal succinimide group with the amine of protein. Following linker deposition, the slides were washed by phosphate buffered saline (PBS) and then rinsed in blocking buffer solution (4 mg mL^{-1} bovine serum albumin, BSA) for 1 h to prevent nonspecific protein binding.

To confirm the effectiveness of device's functionality, the stepwise molecule binding was investigated via monitoring the metasurfaced color and its corresponding reflection spectrum using a motorized stage and a spectrometer coupled to a charge coupled device (CCD) camera (experimental setup as shown in Figure S4, Supporting Information). The sample

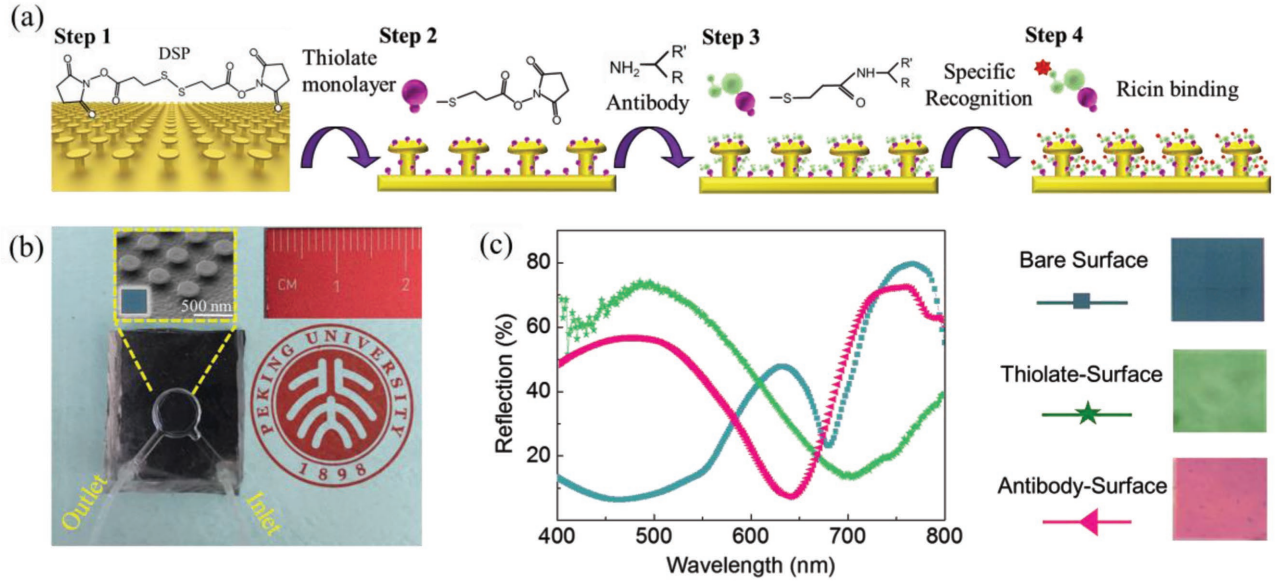

Figure 5. a) Schematic representation of antibody immobilization on plasmonic metasurfaces for ricin visual detection. b) Bright-field microscope photograph of microfluidic channel device. Inset: SEM image of gold nanotexted arrays and their color appearance (scale bar: 500 nm). c) Spectral shift and color changes of the biofunctionalized procedure due to the inter-molecular interaction.

small 2016,
DOI: 10.1002/smll.201601710

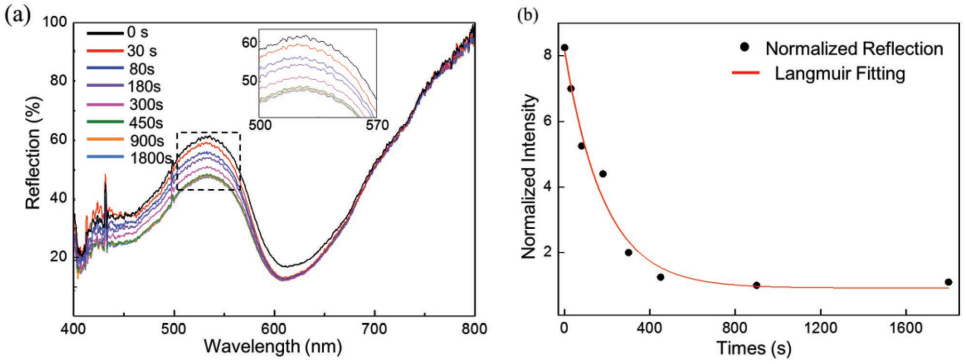

Figure 6. a) Reflection spectra of thiolate-modified PNPMs immersed in buffer during the antiricin binding. The inset is a closeup of the peak and shows a representative response (redshift of the peak) upon antibody adsorption. b) Kinetic plot for antibody immobilization. The response curve was obtained by Langmuir kinetics model fitting at 535 nm.

was rinsed with deionized water and nitrogen drying before each analysis step. From the measured reflection spectra in Figure 5c, we have shown the broadening spectrum linewidth and redshift plasmonic peak during biofunctionalization precedure. The linker-molecular chain of surface modification induces the changed dielectric environment, leading to environment-sensitive plasmon responses. As expected, bouncing color transitions from indigo, green to rose-red were observed.

2.3. Interfacial Kinetics of Antiricin Binding

Plasmonic metasurface biosensing offers facile solution for characterizing biomolecular binding events and their kinetics in real time. It is especially important that binding kinetic analysis provides insights into the mechanism of molecular interactions. Gold nanopin sensing elements integrated in polydimethylsiloxane microfluidic channels were used to monitor antiricin immobilization and measure molecular binding kinetics. 50 µL of 0.1 mg mL^{-1} antiricin solution was injected into microfluidic channel using a syringe pump at a rate of 0.1 mL min^{-1}. Biomolecular binding at the gold surface results in the resonance shift as well as decreased reflection, as shown in **Figure 6**a. The output intensity versus reaction times at 535 nm is plotted in Figure 6b. Our observation suggests that the immobilization process exhibits exponential decay behavior, which is a typical Langmuir kinetics behavior. Langmuir kinetics fitting has been performed and the obtained K_{obs} value is 5.4×10^{-3} s^{-1}, indicating a quick reaction rate of antiricin binding process.

2.4. Sensitivity for Ricin Detection

The target ricin molecule was specifically bond to antibody-modified surface after 10 min incubation. After removal of unbound ricin molecules by rinsing and drying, the reflection spectra were characterized with ricin solutions varying from 10 to 120 ng mL^{-1}, that is shown in **Figure 7**a. It is obvious that the reflection peak becomes broaden and appears red-shift. Figure 7b presents the corresponding colors. A readily identifiable color transition can be observed, ranging from bright rose-red to pale yellow. When we continued to decrease the ricin concentration (<10 ng mL^{-1}) or increase the ricin concentration (>120 ng mL^{-1}), the antiricin surface maintained rose-red for minimum concentration and pale yellow for saturated concentration and there were no recognizable color differences. These results revealed that such nanopin metasurfaces can serve as sensing elements for the visual and quantitative ricin analysis within the range of 10–120 ng mL^{-1}. To experimentally prove ricin specific

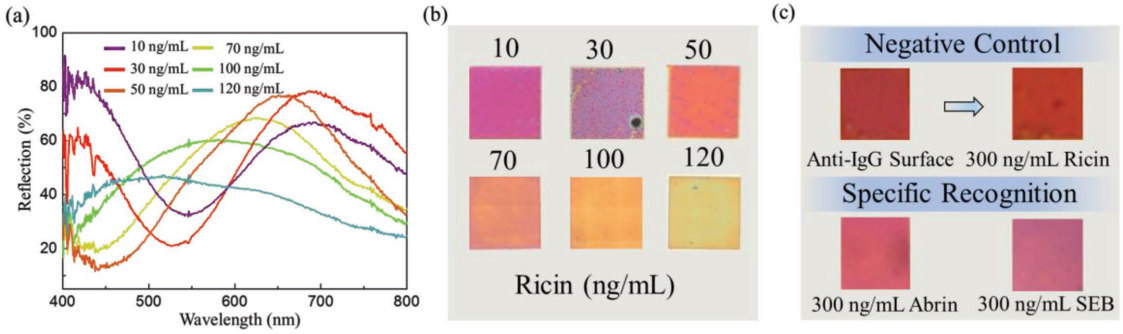

Figure 7. Ricin colorimetric recognition with plasmonic nanopin arrays. a) Reflection spectra of ricin at different concentrations (10–120 ng mL^{-1}) after 10 min immersing in a reaction mixture. The corresponding colorimetric response is shown in (b). Remarkable color changes are due to ricin adherences specifically to the antiricin surface, showing facile and quantitative sensing of ricin. c) Color appearances to study specific recognition utilizing analogs (abrin, SEB) and nonspecific antibody (anti-IgG) functionalized surface. Since there are no special binding affinities, irrelevant antibody or targets fail to produce obvious color changes.

DOI: 10.1002/smll.201601710

recognition, the different target molecules were carefully detected, including abrin and staphylococcus enterotoxin B (SEB) (see Material Selection for Specificity Demonstration in the Supporting Information for further details). In the absence of ricin, these recognition molecules fail to transduce a significant colorimetric signal even at so high concentration of 300 ng mL^{-1}. Negative control experiments were performed using the irrelevant protein (antibody against human immunoglobulin G, Anti-IgG) functionalized metasurfaces to detect 300 ng mL^{-1} ricin. In Figure 7c, the immobilization of anti-IgG on the surface results in amaranth-red appearance. The irrelevant protein (anti-IgG) is not specific for ricin and the ricin even at so high concentration (300 ng mL^{-1}) failed to induce a significant color response. Therefore, this colorimetric sensing system have adequate specificity and sensitivity to detect ricin, which has a the safe dose extent of 350–700 ng mL^{-1} according to the literature recordation.[3]

3. Conclusions

In summary, we have experimentally demonstrated a nanopin-based plasmonic colorimetric sensor for ricin recognition. This 3D nanopin structure can serve as a cavity resonator to induce the electromagnetic energy confinement and standing-wave resonances with narrow bandwidth. In the case of colorimetric sensing applications, these attractive features lead to remarkable color variations. We demonstrate that such colorimetric sensor can be able to quantitatively measure ricin by simply observing the color changes. Furthermore, this engineered colored metasurfaces hold potential in various plasmonic color applications, such as color displays, steganography, and high-density data storage.

4. Experimental Section

Materials: Polyclonal antibody against ricin (antiricin) (0.1 mg mL^{-1}), ricin (1 mg mL^{-1}), abrin (1 mg mL^{-1}), BSA (≥ 98%), antibody against human immunoglobulin G (anti-IgG), and SEB were obtained from Beijing CellChip Biotechnology Co., Ltd. (Beijing, China). DSP (≥ 95%), PBS (10×10^{-6} M, pH 7.4), DMSO were all purchased from Sigma (St. Louis, MO, USA). Hydrogen peroxide (≥30%, guaranteed reagent ≥99.8%) and concentrated sulfuric acid (≥95%–98%, guaranteed reagent ≥99.8%) were received from Beijing Chemical Works (Beijing, China). Aqueous solutions were prepared using water purified at a resistivity of 18.2 MΩ.

Measurement and Simulation: Spectroscopic Measurement, Image Capturing, and Sensing Experiments: Spectral measurements were performed with a Nova spectrophotometer at room temperature using a 1.00 cm quartz cuvette. The measured reflection spectra were normalized with a aluminum mirror reflectance standard ($R > 99\%$). The first data point of kinetic measurements was recorded ≈30 s after solution mixing. Finite element simulations of plasmonic optical response were performed using FDTD method (FDTD solutions, Lumerical Solutions). Based on FDTD analysis, the perfectly matched layer absorbing boundary condition combined with periodic boundary condition was applied for the accurately and efficiently Maxwell's equations.

Supporting Information

Supporting Information is available from the Wiley Online Library or from the author.

Acknowledgements

This work was supported by the National Key Laboratory Foundation, the National Basic Research Program of China (973 Program, Grant No. 2015CB352100), the National Natural Science Foundation of China (Grant No. 61474006) and the Doctoral Program Foundation of State Education Ministry (Grant No. 20130001110007). The authors thank Rui Zhao of Peking University for experimental discussion.

[1] J. Audi, M. Belson, M. Patel, J. Schier, J. Osterloh, *J. Am. Med. Assoc.* **2005**, *294*, 2342.
[2] S. Bradberry, *Medicine* **2012**, *40*, 80.
[3] S. M. Bradberry, K. J. Dickers, P. Rice, G. D. Griffiths, J. A. Vale, *Toxicol. Rev.* **2003**, *22*, 65.
[4] G. D. Griffiths, P. Rice, A. C. Allenby, S.C. Bailey, D. G. Upshall, *Inhalation Toxicol.* **1995**, *7*, 269.
[5] S. Firess, *In Accord, Ricin Owner Enters Plea of Guilty*, *The New York Edition*, America **2008**, p. A18.
[6] F. R. Sidell, E. T. Takafuji, D. R. Franz, *Medical Aspects of Chemical and Biological Warfare*, Office of the Surgeon General (Army), Falls Church, VA **1997**, p. 631.
[7] W. P. Bozza, W. H. Tolleson, L. A. R. Rosado, B. Zhang, *Biotechnol. Adv.* **2015**, *33*, 117.
[8] M. A. Poli, V. R. Rivera, J. F. Hewetson, G. A. Merrill, *Toxicon* **1994**, *32*, 1371.
[9] R. H. Shyu, H. F. Shyu, H. W. Liu, S. S. Tang, *Toxicon* **2002**, *40*, 255.
[10] S. Suresh, M. Gupta, G. A Kumar, V. K. Rao, O. Kumar, P. Ghosal, *Analyst* **2012**, *137*, 4086.
[11] K. Dill, D. D. Montgomery, A. L. Ghindilis, K. R. Schwarzkopf, *Biosens. Bioelectron.* **2004**, *20*, 736.
[12] U. Narang, G. P. Anderson, F. S. Ligler, J. BuransFiber, *Biosens. Bioelectron.* **1997**, *12*, 937.
[13] S. R. Kalb, J. R. Barr, *Anal. Chem.* **2009**, *81*, 2037.
[14] S. C. McGrath, D. M. Schieltz, L. G. McWilliams, J. L. Pirkle, J. R. Barr, *Anal. Chem.* **2011**, *83*, 2897.
[15] V. Guglielmo-Viret, P. Thullier, *J. Immunol. Methods* **2007**, *328*, 70.
[16] B. N. Feltis, B. A. Sexton, F. L. Glenn, M. J. Best, M. Wilkins, T. J. Davis, *Biosens. Bioelectron.* **2008**, *23*, 1131.
[17] G. P. Anderson, R. H. Glaven, W. R. Algar, K. Susumu, M. H. Stewart, I. L. Medintz, E. R. Goldman, *Anal. Chim. Acta* **2013**, *786*, 132.
[18] B. N. Feltis, B. A. Sexton, F. L. Glenn, M. J. Best, M. Wilkins, T. J. Davis, *Biosens. Bioelectron.* **2008**, *23*, 1131.
[19] G. J. Chen, X. H. Ning, B. Park, G. J. Boons, B. Q. Xu, *Langmuir* **2009**, *25*, 2860.
[20] E. A. E. Garber, T. W. O'Brien, *J. AOAC Int.* **2008**, *91*, 376.

DOI: 10.1002/smll.201601710

[21] V. Guglielmo-Viret, P. Thullier, *J. Immunol. Methods* **2007**, *328*, 70.
[22] C. L. Schofield, B. Mukhopadhyay, S. M. Hardy, M. B. McDonnell, R. A. Field, D. A. Russell, *Analyst* **2008**, *133*, 626.
[23] I. Heisler, J. Keller, R. Tauber, M. Sutherland, H. Fuchs, *Anal. Biochem.* **2002**, *302*, 114.
[24] D. L. Brandona, A. M. Korna, L. L. Yanga, *Food Agric. Immunol.* **2014**, *25*, 160.
[25] M. Jiménez, S. André, H. J. Gabius, D. Solísa, *Anal. Biochem.* **2000**, *284*, 418.
[26] J. T. Hu, P. J. Ni, H. C. Dai, Y. J. Sun, Y. L. Wang, S. Jiang, Z. Li, *RSC Adv.* **2015**, *5*, 16036.
[27] J. J. Storhoff, A. D. Lucas, V. Garimella, Y. P. Bao, U. R. Müller, *Nat. Biotechnol.* **2004**, *22*, 883.
[28] M. S. Han, A. K. R. Lytton-Jean, B. K. Oh, J. Heo, C. A. Mirkin, *Angew. Chem., Int. Ed.* **2006**, *45*, 1807.
[29] J. Du, L. Jiang, Q. Shao, X. Liu, R. S. Marks, J. Ma, X. Chen, *Small* **2012**, *9*, 1467.
[30] J. R. Fan, Z. Y. Li, Z. J. Chen, W. G. Wu, *Appl. Surf. Sci.* **2016**, *384*, 534.
[31] C. Chang, Y. F. Wang, Y. Kanamori, J. J. Shih, Y. Kawai, C. K. Lee, K. C. Wu, M. Esashi, *J. Micromech. Microeng.* **2005**, *15*, 580.
[32] C. H. Choi, C. J. Kim, *Nanotechnology* **2006**, *17*, 5326.
[33] Y. H. Gu, F. Qin, J. K. W. Yang, S. P. Yeoa, C. W. Qiu, *Nanoscale* **2014**, *6*, 2106.
[34] H. Lochbihler, Y. Ye, *Opt. Lett.* **2013**, *38*, 1028.
[35] Y. Lim, N. A. Owens, R. D. Wampler, Y. Ying, J. H. Granger, M. D. Porter, *Langmuir* **2014**, *30*, 12868.
[36] D. S. Grubisha, R. J. Lipert, H. Park, J. Driskell, M. D. Porter, *Anal. Chem.* **2003**, *75*, 5936.

Received: May 20, 2016
Revised: August 27, 2016
Published online: